Leukocyte composition of human breast cancer

Brian Ruffell[a], Alfred Au[a,b], Hope S. Rugo[b,c], Laura J. Esserman[b,d], E. Shelley Hwang[b,d], and Lisa M. Coussens[a,b,1]

[a]Department of Pathology and [b]Helen Diller Family Comprehensive Cancer Center, University of California, San Francisco, CA 94143; and Departments of [c]Medicine and [d]Surgery, University of California, San Francisco, CA 94115

Retrospective clinical studies have used immune-based biomarkers, alone or in combination, to predict survival outcomes for women with breast cancer (BC); however, the limitations inherent to immunohistochemical analyses prevent comprehensive descriptions of leukocytic infiltrates, as well as evaluation of the functional state of leukocytes in BC stroma. To more fully evaluate this complexity, and to gain insight into immune responses after chemotherapy (CTX), we prospectively evaluated tumor and nonadjacent normal breast tissue from women with BC, who either had or had not received neoadjuvant CTX before surgery. Tissues were evaluated by polychromatic flow cytometry in combination with confocal immunofluorescence and immunohistochemical analysis of tissue sections. These studies revealed that activated T lymphocytes predominate in tumor tissue, whereas myeloid lineage cells are more prominant in "normal" breast tissue. Notably, residual tumors from an unselected group of BC patients treated with neoadjuvant CTX contained increased percentages of infiltrating myeloid cells, accompanied by an increased CD8/CD4 T-cell ratio and higher numbers of granzyme B-expressing cells, compared with tumors removed from patients treated primarily by surgery alone. These data provide an initial evaluation of differences in the immune microenvironment of BC compared with nonadjacent normal tissue and reveal the degree to which CTX may alter the complexity and presence of selective subsets of immune cells in tumors previously treated in the neoadjuvant setting.

inflammation | macrophage

Several subtypes of CD45-expressing leukocytes infiltrate breast cancer (BC), including CD4$^+$ and CD8$^+$ T cells, CD20$^+$ B cells, and multiple myeloid-lineage cells including tumor-associated macrophages (TAMs) that are often identified by immunohistochemical (IHC) detection of CD68 (1). High lymphocyte infiltration is associated with increased survival in patients <40 y of age (2) and with a favorable prognosis in subsets of patients whose tumors are also heavily infiltrated by TAMs (3). More specifically, large cohort studies of patients with BC have revealed that the presence of CD68$^+$ cells in tumor tissue correlates with poor prognostic features (4–6), higher tumor grade (7–9), increased angiogenesis (10–13), decreased disease-free survival (6, 11, 14, 15), and increased risk for systemic metastasis when assessed in conjunction with endothelial and carcinoma cell markers (16).

The functional significance of specific leukocytes in BC development has been implied based on experimental studies using murine models of mammary carcinogenesis where mice harboring homozygous null mutations in genes specifying leukocyte development or recruitment have been evaluated. In transgenic mice expressing the polyoma virus middle T antigen regulated by the mouse mammary tumor virus promoter (MMTV-PyMT mice), progression of mammary carcinomas and metastases to lungs are reduced in mice lacking the *colony-stimulating factor-1* (*csf1*) gene, a cytokine critical for macrophage maturation and recruitment (17, 18). TAMs in mammary tumor tissue are often associated with vasculature (19), where their production of VEGFA fosters angiogenic programming of tissue (20, 21), and their production of EGF promotes invasive tumor growth and subsequent metastases (22, 23). Moreover, TAMs regulated by epithelial CSF1 express higher levels of several hypoxia-induced genes (*iNOS* and *arginase-1*) that, in turn, mediate suppression of anti-tumor immunity by blocking cytotoxic T-cell proliferation and activation (6, 24). Thus,

TAM presence and bioactivity within mammary tumors correspond to their clinical activity, further indicating the importance of TAMs, not only in promoting tumor development, but also in suppression of anti-tumor immunity.

CD4$^+$ T cells isolated from human BC produce high levels of type II helper (T$_H$2) cytokines including IL-4 and IL-13 (25, 26), which are significant in light of studies demonstrating that several protumor activities of TAMs are regulated by IL-4 derived from CD4$^+$ T cells (1, 27). Based on these findings, we recently reported that infiltration by CD68$^+$, CD4$^+$, and CD8$^+$ immune cells in human BC is predictive of overall survival, and that the ratio of *CD68* to *CD8a* mRNA in tumor tissue correlates with complete pathologic response (pCR) in patients undergoing neoadjuvant chemotherapy (CTX) for early stage BC (6). Despite the clear correlation between these specific immune cell types and BC clinical outcome, leukocyte complexity within tumor tissue remains poorly described, with most studies relying on single-marker IHC detection. Furthermore, although some studies have examined the effects of CTX on the presence and function of circulating peripheral blood leukocytes (28), data regarding the effect of CTX on tumor-infiltrating immune cells are limited (29).

Herein, we evaluated leukocytic infiltrates in breast tissue from predominantly hormone receptor positive patients who had, or had not, received CTX before definitive surgery. In CTX-naïve patients, we found that activated T lymphocytes comprised the majority of immune cells within tumors, whereas myeloid-lineage cells predominate in nonadjacent normal breast tissue. In contrast, tumors from patients with residual disease after neoadjuvant CTX contained higher levels of infiltrating myeloid cells, with a simultaneous shift away from a T$_H$2 dominated lymphocyte response.

Results

Increased Presence of T Cells in Tumor Tissue. To evaluate the composition of tumor-infiltrating leukocytes in human BC, tumors from 20 patients were evaluated by polychromatic flow cytometry and IHC detection of leukocyte lineages in tissue sections as described in *Materials and Methods*. Nine invasive ductal carcinomas (IDC) and five invasive lobular carcinomas (ILC)—mostly histological grade two or three—were obtained from patients with no prior exposure to CTX (CTX-naïve) at the time of primary surgery for early stage BC, although one patient had received neoadjuvant tamoxifen. Six tumor samples were obtained from patients previously treated with neoadjuvant CTX before resection (CTX-treated), consisting entirely of grade two or three IDC. Notably, three of six CTX-treated tumors were HER2/neu-positive, compared with only 1 of 14 CTX-naïve tumors, whereas both groups contained roughly equivalent percentages of tumors negative for estrogen, progesterone, and HER2 receptors (triple negative). Details of tumor pathology are outlined in Table S1. Ipsilateral nonadjacent tissue was also obtained from seven CTX-naïve and four CTX-treated patients

for use as "normal" tissue, in addition to tissues from two contralateral prophylactic mastectomies from patients with ipsilateral ductal carcinoma in situ (DCIS).

Immune infiltrates detected with the pan-leukocyte marker CD45 were present in both normal and tumor tissue, but with substantially increased density in BC (Fig. 1A). Leukocyte subsets were evaluated by using a combination of lineage markers to identify specific subpopulations (Figs. S1 and S2), with the complexity of these populations shown in Fig. 1B as a percentage of the total number of $CD45^+$ cells in each sample. BC tissues from CTX-naïve patients contained infiltrates dominated by T lymphocytes ($CD3\epsilon^+$), with minor populations of natural killer cells ($CD3\epsilon^-CD56^+NKG2D^+$) and B lymphocytes ($CD19/20^+HLA-DR^+CD3^-$). In comparison, myeloid-lineage cells including macrophages ($CD14^{hi}CD11b^+HLA-DR^+$), mast cells ($Fc\epsilon R1\alpha^+CD117^+CD11b^-CD49d^+$) and neutrophils ($CD15^+CD11b^+CD49d^-$) were more evident in the normal tissue from these patients. A similar immune profile was observed in breast tissues obtained from the two prophylactic mastectomies (Fig. 1B).

Increased Presence of Myeloid-Lineage Cells in Residual Tumors from Patients Exposed to Neoadjuvant CTX. Comparative analysis of residual BC tissue removed from patients after neoadjuvant CTX revealed an obvious difference in the percentages of myeloid-lineage cells compared with the CTX-naïve group. With some exceptions, this difference included an increased presence of macrophages as a percent of total leukocytes (Fig. 2A), as well as by density evaluation of CSF1 receptor (CSF1R)-positive cells in tissue by IHC (Fig. 2B). Increased percentages of mast cells (Fig. 2C) and neutrophils (Fig. 2D) were also evident in most CTX-treated patients, with an ≈14-fold increase in CTX-treated versus CTX-naïve groups. Basophils ($Fc\epsilon R1\alpha^+CD117^-CD11b^-CD49d^+$; Fig. 2E) were highly increased in only one of six CTX-treated samples, whereas the percentage of myeloid dendritic cells ($CD11c^+HLA-DR^+CD14^{lo/-}$; Fig. 2F) was unchanged. Evaluation of plasmacytoid dendritic cells expressing CD85g/ILT7 detected an insufficient number of events for analysis. Thus, with the exception of basophils, dendritic cells, and $CD15^+CD11b^+CD49d^+$ eosinophils—which were present just at a detectable level in the tissues examined—increased presence of myeloid-lineage cells typified residual tumors of women treated with neoadjuvant CTX.

CD68 Is Not a Macrophage-Specific Marker in Human BC. Macrophages are well established as regulators of murine mammary tumorigenesis (30), where they can represent up to 80% of leukocytes present within late stage mammary carcinomas (1). In human BC, immunoreactivity for CD68 has been used extensively for identification of macrophages, with $CD68^+$ cell density associated with reduced overall survival (6, 11, 14, 15).

The high number of $CD68^+$ cells reported in the literature, and shown in Fig. 3A, was in contrast to the limited number of $CD14^{hi}CD11b^+HLA-DR^+$ macrophages observed by flow cytometry in the BC suspensions examined (Figs. 1B and 2A). To understand this discrepancy, we first evaluated CD68 expression in BC tissue sections, compared with CD163 (a hemoglobin scavenger receptor also commonly used as a marker for macrophages) and CSF1R (Fig. 3A). This comparative analysis revealed a lack of correlation in cell density among the three markers. We next evaluated frozen BC tissue sections by confocal microscopy after immunofluorescent detection of CD68 in combination with CSF1R or CD45 (Fig. 3B). Although all cells expressing high levels of the CSF1R also expressed CD68, there was a distinct population of $CD68^+$ cells that expressed neither CSF1R nor CD45. CD68 did not significantly colocalize with keratin$^+$ epithelial cells, $CD31^+$ endothelial cells, or smooth muscle actin α-expressing mural cells surrounding vasculature (Fig. 3C). This expression contrasted with murine mammary tumors isolated from MMTV-PyMT transgenic mice (17), where $CD68^+$ cells coexpressed both CSF1R and the murine macrophage marker F4/80 (Fig. S3). In agreement with historic literature (31, 32), these results thus indicate that CD68 is not a macrophage-specific marker in human BC.
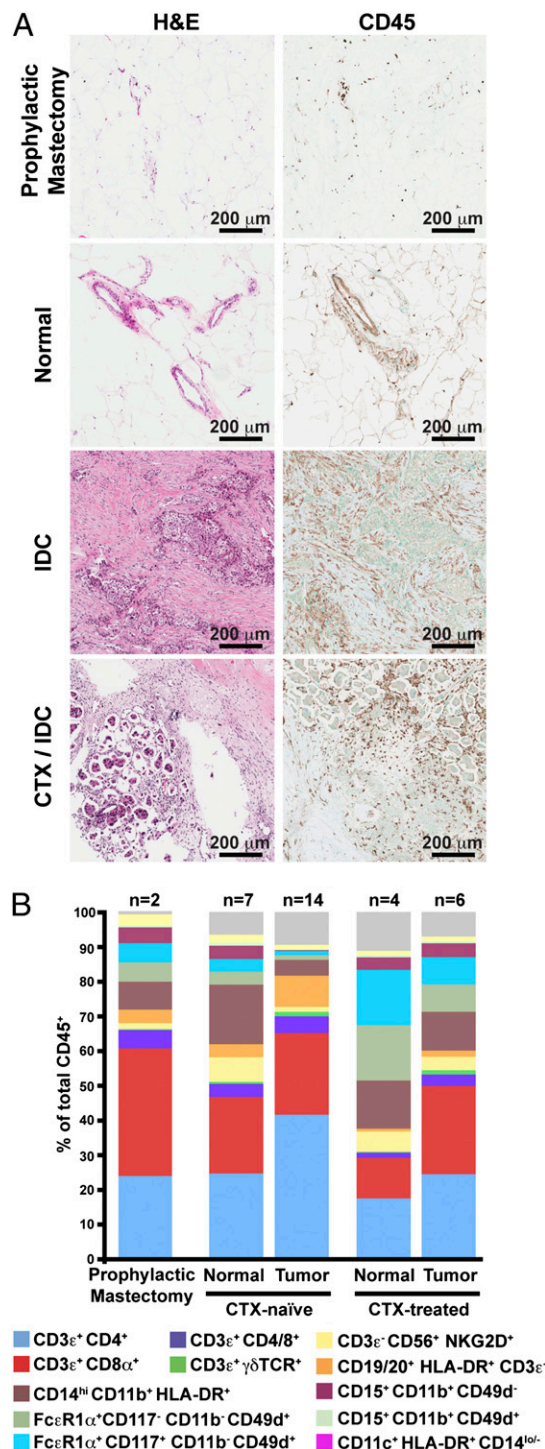
Fig. 1. Leukocyte infiltration of human breast tumors. (A) Hematoxylin and eosin (H&E) staining of tissue sections (*Left*) with representative immunohistochemistry for CD45 (*Right*) shown for each. (B) Flow cytometric analysis of leukocyte populations within human breast tumors. Results are shown as a percent of total $CD45^+$ cells with markers used to define specific lineages shown below.

Tumor-Infiltrating T Cells Display an Activated Phenotype. To reveal the phenotype of T cells infiltrating BCs, we examined surface marker and chemokine receptor expression of tissue-infiltrating $CD4^+$ and $CD8^+$ T cells (Fig. 4 A and B). Specifically, both $CD4^+$ and $CD8^+$ T cells displayed increased expression of activation markers CD69 and HLA-DR compared with peripheral

Fig. 2. Increased myeloid-lineage leukocyte infiltration within CTX-treated patients. (*A*) CD14^{hi}CD11b$^+$HLA-DR$^+$ macrophages shown as a percent of total CD45$^+$ cells as determined by flow cytometry. (*B*) Representative immunohistochemistry for CSF1R in tumors from either CTX-naïve (*Upper*) or CTX-trea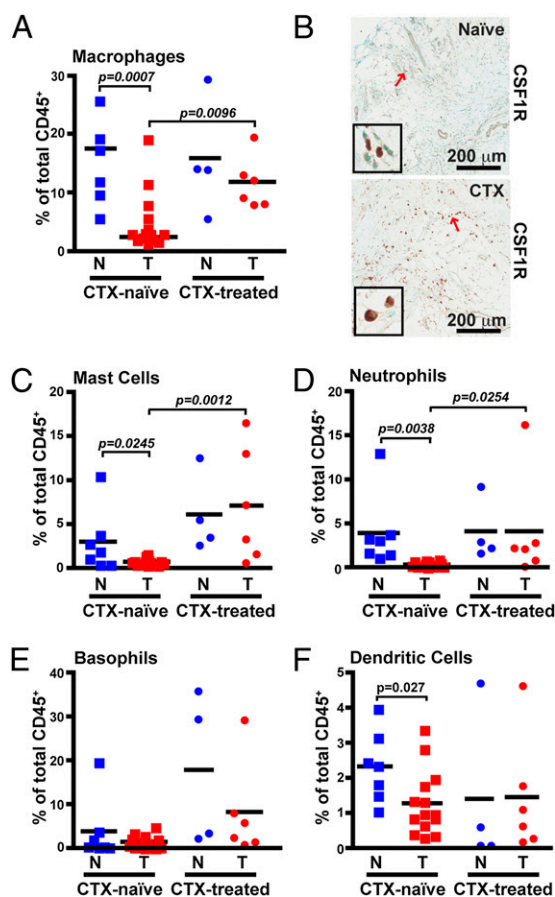ted (*Lower*) patients. Red arrows indicate cells displayed in enlarged insets. FcεR1α$^+$CD117$^+$CD11b$^-$CD49d$^+$ mast cells (*C*), CD15$^+$CD11b$^+$CD49d$^-$ neutrophils (*D*), FcεR1α$^+$CD117$^-$CD11b$^-$CD49d$^+$ basophils (*E*), and CD11c$^+$HLA-DR$^+$CD14$^{lo/-}$ (*F*) DCs shown as a percent of total CD45$^+$ cells. N, nonadjacent normal; T, tumor.

blood T cells, with a corresponding loss of markers for naïve T cells, CD45RA, and CCR7. Furthermore, although all T cells constitutively expressed the costimulatory receptor CD28 (Fig. S4*A*), expression of CD27, another costimulatory receptor, was reduced in a large proportion of tissue-infiltrating cells, indicative of shedding after interaction with its ligand CD70 (33) and potential acquisition of effector functions (34, 35). CD4$^+$ and CD8$^+$ T cells also displayed substantially up-regulated expression of chemokine receptors CCR4 and CCR5 (Fig. 4*B*), and although CD8$^+$ T cells constitutively expressed CXCR3, tissue-infiltrating CD4$^+$ T cells exhibited higher CXCR3 expression than their counterparts in peripheral blood. Surface marker expression by tissue-infiltrating CD4$^+$ and CD8$^+$ T cells was subtly different between tumor and benign tissue in some samples; however, these changes were not consistent across patients, or between CTX-naïve and CTX-treated groups (Fig. S4*B*).

Altered Lymphocyte Balance in Residual Tumors After Neoadjuvant CTX. Although we observed no difference in the percent of CD3e$^-$CD56$^+$NKG2D$^+$ natural killer (NK) cells (Fig. 5*A*), higher levels of CD19/CD20$^+$HLA-DR$^+$ B cells were evident in several CTX-naïve tumors compared with both normal tissue and CTX-treated tumors. As has been reported (36), B cells were clustered together in association with T cells (Fig. 5*C*). Notably, CD4$^+$ T cells as a percent of the total CD45$^+$ pop-
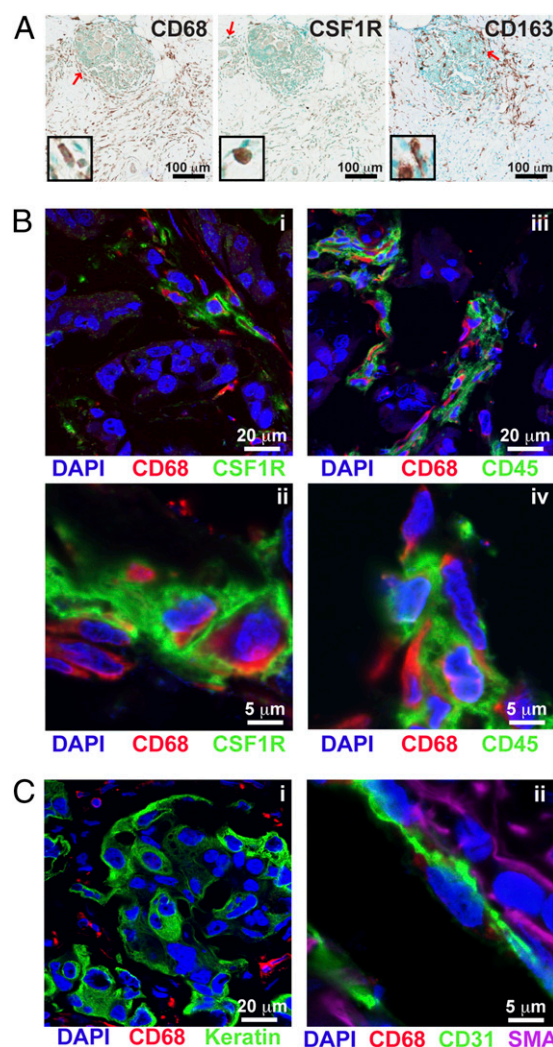

Fig. 3. CD68 is not a specific macrophage marker in human breast tumor tissue. (*A*) Representative immunohistochemistry within tumors for CD68 (*Left*), CSF1R (*Center*), and CD163 (*Right*) in serial sections from a CTX-treated patient. Red arrows indicate cells displayed in enlarged insets. (*B*) Immunofluorescent staining of human breast tumors for CD68 (red) in conjunction with CSF1R (*i* and *ii*) or CD45 (*iii* and *iv*). (*C*) Immunofluorescent staining for CD68 (red) in conjunction with pan-keratin (green; *i*), or CD31 (green) and smooth muscle actin-α (SMA; purple; *ii*).

ulation were also increased in CTX-naïve tumors compared with both normal tissue and residual postneoadjuvant tumors (Fig. 5*D*). As the percent of CD8$^+$ T cells was unchanged (Fig. 5*E*), the lower percentage of CD4$^+$ T cells within the CTX-treated group resulted in an increased CD8 to CD4 ratio (Fig. 5*F*). Although it was unclear whether the density of CD8$^+$ cells in CTX-treated residual tumors was increased (Fig. 5*G*), the number of cells expressing granzyme B was strikingly evident in two of six CTX-treated tumors (Fig. 5*H*), whereas minimal granzyme B staining was observed in CTX-naïve tumors, even in areas with high numbers of CD8$^+$ T cells (Fig. 5*I*).

Despite the reduced percentage of CD4$^+$ T cells in tumors from CTX-treated patients, there was no change in the density of IHC detected regulatory T cells expressing FoxP3 (Fig. S5*A*), which was specifically expressed by CD3$^+$CD4$^+$ cells in the tumor (Fig. S5*B*). Gating on CD25^{hi} cells, consisting of >80% FoxP3$^+$ cells in all samples tested, also revealed that the relative percentage of these cells was invariant between groups (Fig. S5*C*). Phenotypically, CD4$^+$FoxP3$^+$ cells displayed an activated phenotype with equivalent surface levels of CD45RO and CD69
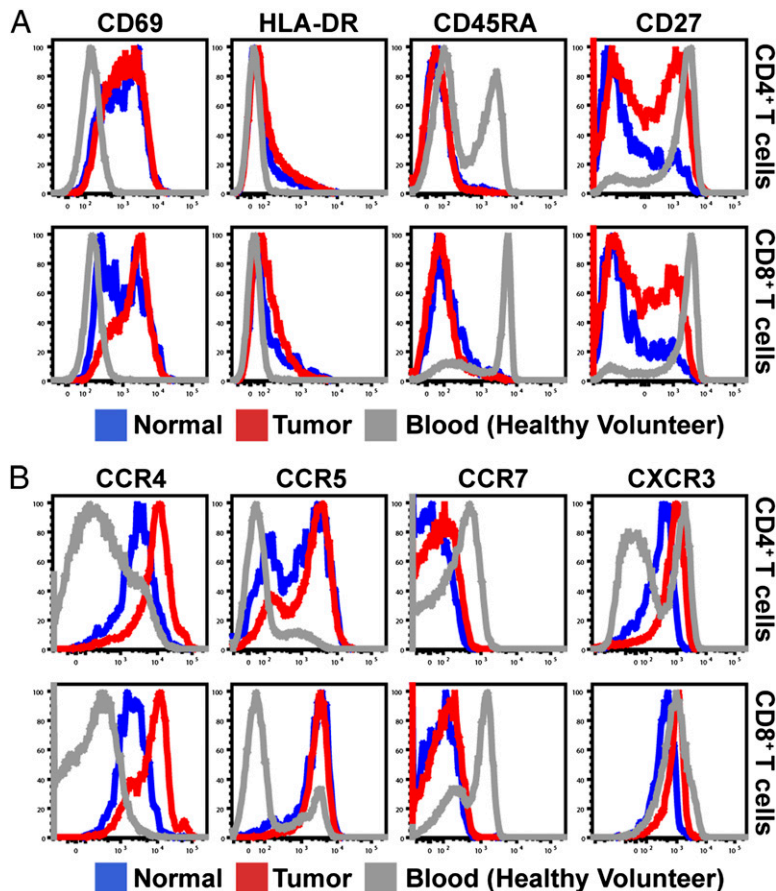
Fig. 4. Tissue-infiltrating T cells display an activated phenotype. (*A* and *B*) Representative histograms of CD3$^+$CD4$^+$ (*Upper*) or CD3$^+$CD8$^+$ (*Lower*) T cells isolated from a single CTX-treated patient with both normal (blue) and tumor (red) tissue. Expression of activation markers CD69 (*Left*), HLA-DR (*Center Left*), CD45RA (*Center Right*), and CD27 (*Right*) are shown in *A*, and expression of chemokine receptors CCR4 (*Left*), CCR5 (*Center Left*), CCR7 (*Center Right*) and CXCR3 (*Right*) are shown in *B*.

to CD4$^+$FoxP3$^-$ cells and, as has been reported for cells in peripheral blood (37), expressed lower levels of CD127 (Fig. S5*D*). Interestingly, although not all FoxP3$^+$ cells expressed HLA-DR, they did comprise the majority of HLA-DR–expressing CD4$^+$ T cells, in addition to coexpressing high levels of CD25.

These data collectively reveal a shift within tumors toward a T$_H$2-type response in BC characterized by increased presence of B cells and CD4$^+$ T cells, in comparison with nonadjacent normal breast tissue. This shift is reversed in tumors obtained from CTX-treated patients, with additional evidence of a cytotoxic T-cell response through a more favorable CD8/CD4 T-cell ratio and increased presence of granzyme B-expressing lymphocytes; thus, even residual tumors from patients with a poor response to CTX may contain immune microenvironments that are more favorably skewed towards an anti-tumor, T$_H$1-type immune response.

Discussion

Herein, we present a detailed description of leukocyte complexity in BC as evaluated in a cohort of CTX-naïve patients with stage 2/3 tumors, compared with patients with significant residual disease after neoadjuvant CTX. T lymphocytes were the major population within both CTX-naïve and CTX-treated tumors, found almost exclusively in an activated state as determined by increased expression of CD69 and chemokine receptors, with simultaneous loss of naïve markers CCR7 and CD45RA. The presence of activation markers, however, does not definitively demonstrate that intratumoral T cells are functionally active. In fact, granzyme B expression was minimal within tumors from CTX-naïve patients, suggesting negligible cytotoxic activity by infiltrating CD8$^+$ T cells. In comparison, granzyme B was highly expressed in one-third of the CTX-treated tumors, suggestive of a more cytotoxic T-cell response within some tumors after exposure to CTX.

Importantly, residual tumors from CTX-treated patients also contained reduced percentages of B cells and CD4$^+$ T cells. Tumor-infiltrating CD4$^+$ T cells in BC are known to express the T$_H$2 cytokines IL-4 and IL-13 concomitantly with the production of IFN-γ (25, 26), consistent with coexpression of CXCR3 and CCR4 (38, 39) as we observed herein. It remains to be determined whether cytokine production by CD4$^+$ T cells is altered by neoadjuvant CTX; however, the combined reduction in both CD4$^+$ T cells and B cells is indicative of a favorable shift away from a T$_H$2 microenvironment. This shift could be relevant for TAM function, as has been described in the MMTV-PyMT model where TAMs are programmed by IL-4 toward a T$_H$2 phenotype (1), and more recently in pancreatic ductal adenocarcinoma during treatment where an agonist CD40 monoclonal antibody fostered cytolytic macrophage activities (40).

Although the extent of lymphocyte infiltration has been associated with improved prognosis in subsets of patients (2, 3), and with pCR after CTX (41, 42), information regarding the relationship between individual lymphocyte subsets to survival is limited. High FoxP3 counts correlate with reduced overall and relapse-free survival in estrogen receptor (ER)-positive tumors (43), and pCR to neoadjuvant CTX is associated with reduced FoxP3 grading (44, 45). Although two studies examining T-cell infiltration by flow cytometry found conflicting results regarding the CD8:CD4 ratio and lymph node metastasis (46, 47), the number of CD8$^+$ T cells within tissue has been associated with improved patient survival (48). We have also reported a CD68/CD4/CD8 immune signature predicting overall and relapse-free survival, with inverse correlations evident for CD4 when used in conjunction with other markers (6). There is thus an urgent need for additional prospective investigations where multiple parameters of lymphocytic infiltration and functionality are evaluated to determine the most significant biomarker comparisons that predict outcome and guide specific therapy.
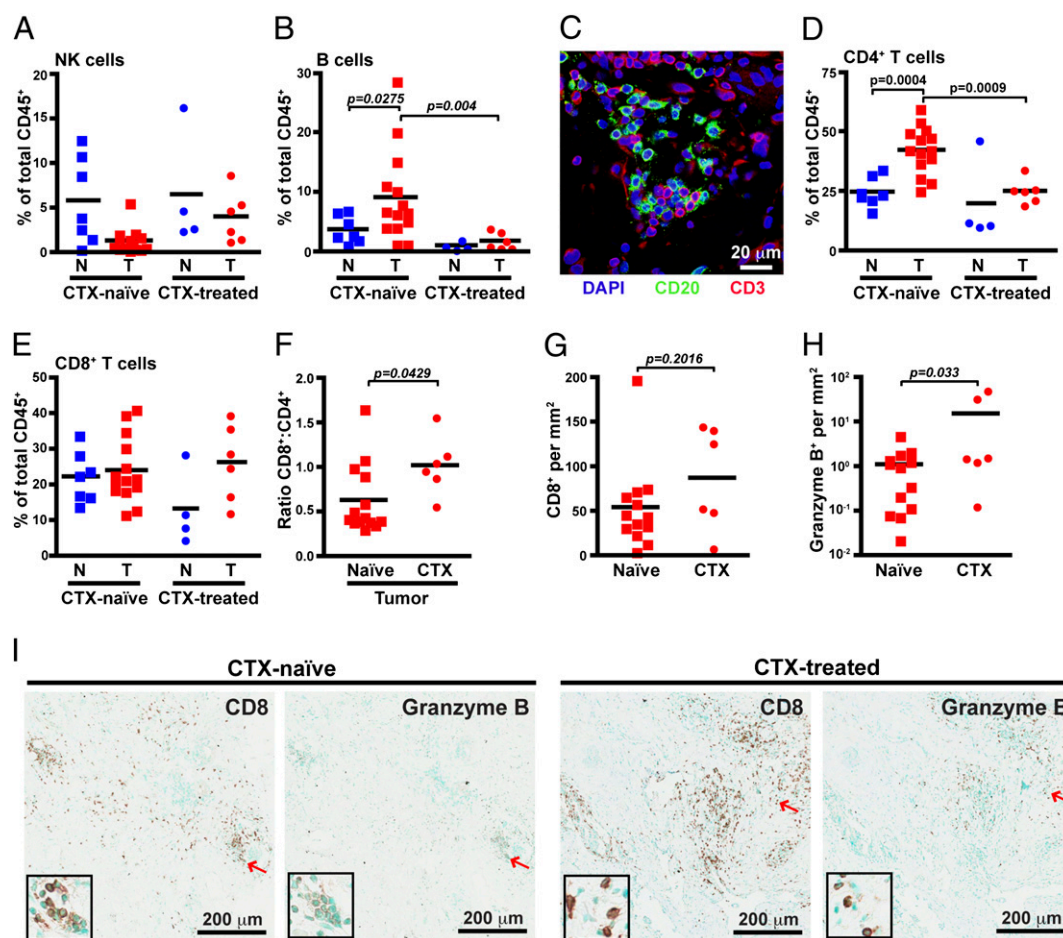
Fig. 5. Improved cytotoxic T-cell response in CTX-treated tumors. CD3ε⁻CD56⁺NKG2D⁺ natural killer cells (*A*) and CD3ε⁻CD19/20⁺HLA-DR⁺ B cells (*B*) shown as a percent of total CD45⁺ cells as determined by flow cytometry. (*C*) Immunofluorescent staining of tumors for CD20 (green) and CD3 (red). CD3ε⁺CD4⁺ T cells (*D*) and CD3ε⁺CD8⁺ T cells (*E*) are shown as a percent of total CD45⁺ cells. (*F*) Ratio of CD8⁺ to CD4⁺ T cells within CTX-naive versus CTX-treated tumors. Number of CD8-positive (*G*) and granzyme B-positive (*H*) cells per area as determined by automated counting. (*I*) Representative sections stained with CD8 or granzyme B from CTX-naive (*Left*) or CTX-treated (*Right*) tumors. Red arrows indicate cells displayed in enlarged insets. N, nonadjacent normal; T, tumor.

Although used successfully in multiple studies to relate TAM infiltration with clinically relevant outcomes, our results indicate that CD68 alone cannot accurately evaluate macrophage presence in human breast tissue given that multiple stromal cells express it and that a subset of these are CSF1R- and CD45-negative. We observed that the nonleukocytic CD68⁺ cells were predominantly located within tumor stroma and, thus, based on this localization and morphology, we speculate that CSF1R⁻CD68⁺ cells likely reflect tumor-associated fibroblasts or monocyte-derived fibrocytes in agreement with other reports (31, 32, 49–52). Our findings do not invalidate CD68 as a clinically relevant marker and, importantly, CSF1-response gene signatures have been identified in breast adenocarcinomas that are predictive of recurrence risk and metastasis (53, 54). However, given the important role that fibroblasts (and perhaps fibrocytes) play in fostering aspects of tumorigenesis (55–57), differentiating among macrophages, fibroblasts, and other stromal populations within tumors has the potential to improve diagnostic information currently generated by immunodetection of CD68.

As we have reported for expression of *csf1* mRNA (6), multiple genes encoding myeloid cell chemoattractants are differentially expressed by human BC cell lines, with variable induction of these genes in response to CTX (Fig. S6). Although differential expression between cell lines corresponding to particular subtypes of BC is evident, it is doubtful these cell lines accurately represent the response of BC tumor tissue; thus, we are investigating whether differences in myeloid cell infiltrates

reflect distinct molecular subtypes of BC and to what extent these differ in residual tumors from CTX-treated patients.

It is important to acknowledge that leukocyte composition within tumors responding to CTX likely differs substantially from residual or recurrent tumors from patients that have received CTX, given what is known regarding immune responses to CTX-induced cell death (28). However, we recently reported that in mammary carcinomas of MMTV-PyMT mice, blockade of the CSF1-CSF1R pathway critical for TAM recruitment improved response to CTX through a CD8⁺ T-cell–dependent effect (6). Thus, even though the findings presented herein are based on a small dataset of heterogeneous tumor subtypes, and our results may be biased because of sample selection favoring large and/or less CTX-responsive tumors among the CTX-treated group, the clear distinctions in the myeloid profiles between CTX-naive and CTX-treated tumors is provocative and indicates that a CSF1-targeted strategy may be a promising approach to enhance therapeutic efficacy of cytotoxic CTX, particularly for treatment of refractory BC. Moreover, given the increase in granulocytic populations within tumors resistant to CTX, and the involvement of these cells in regulating immune responses in chronic inflammatory diseases (58–62), these populations may also be functionally relevant, and targeting common pathways of immune suppression within the tumor microenvironment may provide additional therapeutic opportunities to increase efficacy of neoadjuvant CTX.

Materials and Methods

Tissues were collected at the time of surgery from consenting patients at the University of California, San Francisco under approval from the institutional review board. Tumor and ipsilateral nonadjacent normal tissues were collected by a certified pathologist (A.A.) and were prepared for analysis on the day of resection. The percent of macrophages and CD8^{+} T cells has been reported for a subset of the patients described here (6). Flow cytometry, immunohistochemistry, and immunofluorescence were performed as described (6), with detailed methods contained in *SI Materials and Methods*, and a list of antibodies available in Tables S2 and S3. Statistical differences between two independent groups were determined by using Student's *t* test via Prism 4.0 software (GraphPad Software).

1. DeNardo DG, et al. (2009) CD4(+) T cells regulate pulmonary metastasis of mammary carcinomas by enhancing protumor properties of macrophages. *Cancer Cell* 16:91–102.
2. Ménard S, et al. (1997) Lymphoid infiltration as a prognostic variable for early-onset breast carcinomas. *Clin Cancer Res* 3:817–819.
3. Pupa SM, et al. (1996) Macrophage infiltrate and prognosis in c-erbB-2-overexpressing breast carcinomas. *J Clin Oncol* 14:85–94.
4. Bingle L, Brown NJ, Lewis CE (2002) The role of tumour-associated macrophages in tumour progression: Implications for new anticancer therapies. *J Pathol* 196:254–265.
5. Mukhtar RA, Nseyo O, Campbell MJ, Esserman LJ (2011) Tumor-associated macrophages in breast cancer as potential biomarkers for new treatments and diagnostics. *Expert Rev Mol Diagn* 11:91–100.
6. DeNardo DG, et al. (2011) Leukocyte complexity in breast cancer predicts overall survival and functionally regulates response to chemotherapy. *Cancer Discovery* 1:54–67.
7. Esserman LJ, et al. (2006) Magnetic resonance imaging captures the biology of ductal carcinoma in situ. *J Clin Oncol* 24:4603–4610.
8. Volodko N, Reiner A, Rudas M, Jakesz R (1998) Tumour-associated macrophages in breast cancer and their prognostic correlations. *Breast* 7:99–105.
9. Lee AH, Happerfield LC, Bobrow LG, Millis RR (1997) Angiogenesis and inflammation in invasive carcinoma of the breast. *J Clin Pathol* 50:669–673.
10. Uzzan B, Nicolas P, Cucherat M, Perret GY (2004) Microvessel density as a prognostic factor in women with breast cancer: A systematic review of the literature and meta-analysis. *Cancer Res* 64:2941–2955.
11. Tsutsui S, et al. (2005) Macrophage infiltration and its prognostic implications in breast cancer: The relationship with VEGF expression and microvessel density. *Oncol Rep* 14:425–431.
12. Bolat F, et al. (2006) Microvessel density, VEGF expression, and tumor-associated macrophages in breast tumors: Correlations with prognostic parameters. *J Exp Clin Cancer Res* 25:365–372.
13. Chen JJ, et al. (2005) Tumor-associated macrophages: The double-edged sword in cancer progression. *J Clin Oncol* 23:953–964.
14. Leek RD, et al. (1996) Association of macrophage infiltration with angiogenesis and prognosis in invasive breast carcinoma. *Cancer Res* 56:4625–4629.
15. Campbell MJ, et al. (2010) Proliferating macrophages associated with high grade, hormone receptor negative breast cancer and poor clinical outcome. *Breast Cancer Res Treat* 128:703–711.
16. Robinson BD, et al. (2009) Tumor microenvironment of metastasis in human breast carcinoma: A potential prognostic marker linked to hematogenous dissemination. *Clin Cancer Res* 15:2433–2441.
17. Guy CT, Cardiff RD, Muller WJ (1992) Induction of mammary tumors by expression of polyomavirus middle T oncogene: A transgenic mouse model for metastatic disease. *Mol Cell Biol* 12:954–961.
18. Lin EY, Nguyen AV, Russell RG, Pollard JW (2001) Colony-stimulating factor 1 promotes progression of mammary tumors to malignancy. *J Exp Med* 193:727–740.
19. Lin EY, et al. (2006) Macrophages regulate the angiogenic switch in a mouse model of breast cancer. *Cancer Res* 66:11238–11246.
20. Stockmann C, et al. (2008) Deletion of vascular endothelial growth factor in myeloid cells accelerates tumorigenesis. *Nature* 456:814–818.
21. Lin EY, et al. (2007) Vascular endothelial growth factor restores delayed tumor progression in tumors depleted of macrophages. *Mol Oncol* 1:288–302.
22. Wyckoff J, et al. (2004) A paracrine loop between tumor cells and macrophages is required for tumor cell migration in mammary tumors. *Cancer Res* 64:7022–7029.
23. Wyckoff JB, et al. (2007) Direct visualization of macrophage-assisted tumor cell intravasation in mammary tumors. *Cancer Res* 67:2649–2656.
24. Doedens AL, et al. (2010) Macrophage expression of hypoxia-inducible factor-1 alpha suppresses T-cell function and promotes tumor progression. *Cancer Res* 70:7465–7475.
25. Aspord C, et al. (2007) Breast cancer instructs dendritic cells to prime interleukin 13-secreting CD4+ T cells that facilitate tumor development. *J Exp Med* 204:1037–1047.
26. Pedroza-Gonzalez A, et al. (2011) Thymic stromal lymphopoietin fosters human breast tumor growth by promoting type 2 inflammation. *J Exp Med* 208:479–490.
27. Gocheva V, et al. (2010) IL-4 induces cathepsin protease activity in tumor-associated macrophages to promote cancer growth and invasion. *Genes Dev* 24:241–255.
28. Zitvogel L, Apetoh L, Ghiringhelli F, Kroemer G (2008) Immunological aspects of cancer chemotherapy. *Nat Rev Immunol* 8:59–73.
29. Allan CP, Turtle CJ, Mainwaring PN, Pyke C, Hart DN (2004) The immune response to breast cancer, and the case for DC immunotherapy. *Cytotherapy* 6:154–163.
30. Qian BZ, Pollard JW (2010) Macrophage diversity enhances tumor progression and metastasis. *Cell* 141:39–51.
31. Pulford KA, Sipos A, Cordell JL, Stross WP, Mason DY (1990) Distribution of the CD68 macrophage/myeloid associated antigen. *Int Immunol* 2:973–980.
32. Kunz-Schughart LA, et al. (2003) [The "classical" macrophage marker CD68 is strongly expressed in primary human fibroblasts]. *Verh Dtsch Ges Pathol* 87:215–223.
33. Hintzen RQ, et al. (1994) Characterization of the human CD27 ligand, a novel member of the TNF gene family. *J Immunol* 152:1762–1773.
34. Hamann D, et al. (1997) Phenotypic and functional separation of memory and effector human CD8+ cells. *J Exp Med* 186:1407–1418.
35. Okada R, Kondo T, Matsuki F, Takata H, Takiguchi M (2008) Phenotypic classification of human CD4+ T cell subsets and their differentiation. *Int Immunol* 20:1189–1199.
36. Nelson BH (2010) CD20+ B cells: The other tumor-infiltrating lymphocytes. *J Immunol* 185:4977–4982.
37. Liu W, et al. (2006) CD127 expression inversely correlates with FoxP3 and suppressive function of human CD4+ T reg cells. *J Exp Med* 203:1701–1711.
38. Kunkel EJ, et al. (2002) Expression of the chemokine receptors CCR4, CCR5, and CXCR3 by human tissue-infiltrating lymphocytes. *Am J Pathol* 160:347–355.
39. Kim CH, et al. (2001) Rules of chemokine receptor association with T cell polarization in vivo. *J Clin Invest* 108:1331–1339.
40. Beatty GL, et al. (2011) CD40 agonists alter tumor stroma and show efficacy against pancreatic carcinoma in mice and humans. *Science* 331:1612–1616.
41. Demaria S, et al. (2001) Development of tumor-infiltrating lymphocytes in breast cancer after neoadjuvant paclitaxel chemotherapy. *Clin Cancer Res* 7:3025–3030.
42. Denkert C, et al. (2010) Tumor-associated lymphocytes as an independent predictor of response to neoadjuvant chemotherapy in breast cancer. *J Clin Oncol* 28:105–113.
43. Bates GJ, et al. (2006) Quantification of regulatory T cells enables the identification of high-risk breast cancer patients and those at risk of late relapse. *J Clin Oncol* 24:5373–5380.
44. Ladoire S, et al. (2008) Pathologic complete response to neoadjuvant chemotherapy of breast carcinoma is associated with the disappearance of tumor-infiltrating foxp3+ regulatory T cells. *Clin Cancer Res* 14:2413–2420.
45. de Kruijf EM, et al. (2010) The predictive value of HLA class I tumor cell expression and presence of intratumoral Tregs for chemotherapy in patients with early breast cancer. *Clin Cancer Res* 16:1272–1280.
46. Macchetti AH, et al. (2006) Tumor-infiltrating CD4+ T lymphocytes in early breast cancer reflect lymph node involvement. *Clinics (Sao Paulo)* 61:203–208.
47. Sheu BC, et al. (2008) Clinical significance of tumor-infiltrating lymphocytes in neoplastic progression and lymph node metastasis of human breast cancer. *Breast* 17:604–610.
48. Mahmoud SM, et al. (2011) Tumor-infiltrating CD8+ lymphocytes predict clinical outcome in breast cancer. *J Clin Oncol* 29:1949–1955.
49. Gottfried E, et al. (2008) Expression of CD68 in non-myeloid cell types. *Scand J Immunol* 67:453–463.
50. Pilling D, Fan T, Huang D, Kaul B, Gomer RH (2009) Identification of markers that distinguish monocyte-derived fibrocytes from monocytes, macrophages, and fibroblasts. *PLoS ONE* 4:e7475.
51. Shao DD, Suresh R, Vakil V, Gomer RH, Pilling D (2008) Pivotal Advance: Th-1 cytokines inhibit, and Th-2 cytokines promote fibrocyte differentiation. *J Leukoc Biol* 83:1323–1333.
52. Azambuja D, et al. (May 2, 2011) Lack of association of tumor-associated macrophages with clinical outcome in patients with classical Hodgkin's lymphoma. *Ann Oncol*, 10.1093/annonc/mdr157.
53. Sharma M, et al. (2010) Analysis of stromal signatures in the tumor microenvironment of ductal carcinoma in situ. *Breast Cancer Res Treat* 123:397–404.
54. Beck AH, et al. (2009) The macrophage colony-stimulating factor 1 response signature in breast carcinoma. *Clin Cancer Res* 15:778–787.
55. Trimboli AJ, et al. (2009) Pten in stromal fibroblasts suppresses mammary epithelial tumours. *Nature* 461:1084–1091.
56. Erez N, Truitt M, Olson P, Arron ST, Hanahan D (2010) Cancer-associated fibroblasts are activated in incipient neoplasia to orchestrate tumor-promoting inflammation in an NF-kappaB-dependent manner. *Cancer Cell* 17:135–147.
57. Kalluri R, Zeisberg M (2006) Fibroblasts in cancer. *Nat Rev Cancer* 6:392–401.
58. Schmielau J, Finn OJ (2001) Activated granulocytes and granulocyte-derived hydrogen peroxide are the underlying mechanism of suppression of T-cell function in advanced cancer patients. *Cancer Res* 61:4756–4760.
59. Fridlender ZG, et al. (2009) Polarization of tumor-associated neutrophil phenotype by TGF-beta: "N1" versus "N2" TAN. *Cancer Cell* 16:183–194.
60. Eller K, et al. (2011) IL-9 production by regulatory T cells recruits mast cells that are essential for regulatory T cell-induced immune suppression. *J Immunol* 186:83–91.
61. Galli SJ, Nakae S, Tsai M (2005) Mast cells in the development of adaptive immune responses. *Nat Immunol* 6:135–142.
62. Perrigoue JG, et al. (2009) MHC class II-dependent basophil-CD4+ T cell interactions promote T(H)2 cytokine-dependent immunity. *Nat Immunol* 10:697–705.

Supporting Information

Ruffell et al. 10.1073/pnas.1104303108

SI Materials and Methods

Flow Cytometry. Freshly resected tissue was manually minced and then incubated for 45 min at 37 °C in DMEM (Invitrogen) with 2.0 mg/mL Collagenase A (Roche) and 50 units/mL DNase I (Roche). Single cell suspensions were prepared by filtering through 70-μm nylon strainers (BD Biosciences), and $<10^6$ cells were incubated for 30 min on ice with Fc Receptor Binding Inhibitor (eBioscience) diluted 1/10 in PBS containing Live Dead Aqua (1:500, Invitrogen). Cells were then incubated for 30 min in PBS containing 1.0 mM EDTA and 5% FCS along with manufacturers' suggested dilutions of fluorescently labeled primary monoclonal antibodies (Table S2). After washing once, cells were fixed with BD Cytofix for 30 min on ice, washed again, and stored at 4 °C until analysis with an LSRII flow cytometer (BD Bioscience). Before intracellular FoxP3 staining, cells were instead fixed with the FoxP3 Fixation/Permeabilization system (eBioscience) according to the manufacturer's instructions.
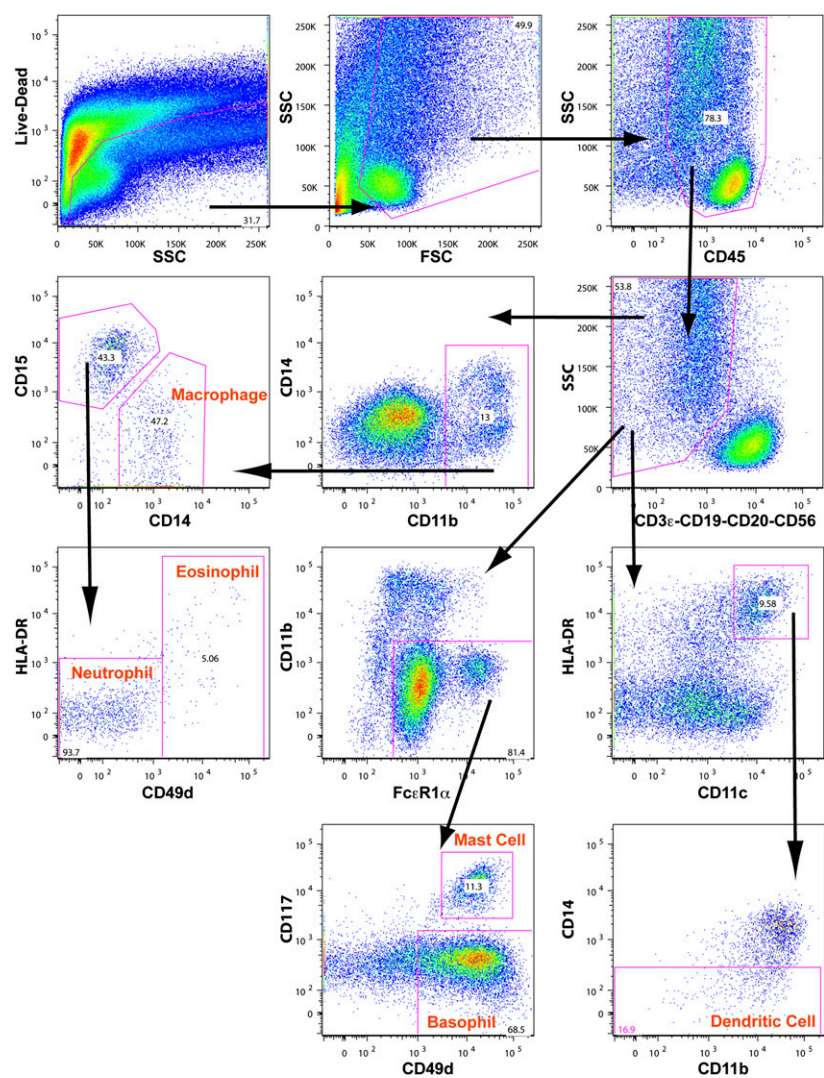
Immunohistochemistry. Sections (5 μm) of formalin-fixed, paraffin-embedded tissues were deparaffinized with xylene, rehydrated, immersed in antigen retrieval citra (BioGenex), then heated for 7 min at maximum power in a microwave, followed by a 30-min incubation in the heated buffer. After washing 3 times in PBS and surrounding tissues with a hydrophobic Super Pap Pen (The Binding Site), peroxidase activity and nonspecific binding was blocked with appropriate components of the Thermo Scientific Ultravision Detection Kit according to the manufacturer's instructions. After a second blocking step with PBS containing 5% goat serum, 2.5% BSA, and 0.1% Tween-20, unlabeled primary antibodies (Table S3) were diluted according to manufacturers' recommendations and added to sections overnight at 4 °C. After washing, antibodies were detected by using the appropriate components of the Thermo Scientific Ultravision Detection Kit according to manufacturer's instructions. After development with liquid DAB, slides were washed in H_2O, counterstained briefly with 1% Methyl Green, dehydrated, and mounted with Cytoseal (Thermo Scientific). Representative images and quantitative image analysis was done by using the Aperio ScanScope CS Slide Scanner (Aperio Technologies) system with a 20× or 40× objective to capture whole-slide images. Positive staining was assessed with the nuclear default algorithm (Aperio).

Immunofluorescence. Sections (10 μm) of PFA fixed, sucrose protected, OCT embedded tissues were thawed at 37 °C for 10 min, permeabilized with 100% ice-cold acetone for 10 min, washed in PBS, and then blocked with goat blocking buffer for 2 h. To use two primary antibodies from the same species, one antibody was added at a 100-fold reduced dilution overnight at 4 °C in 0.5× blocking buffer, and after washing, slides were incubated with a biotinylated anti-mouse or rabbit secondary (Vector Laboratories) for 30 min. The signal from the diluted antibody was then amplified with a TSA indirect kit (Perkin-Elmer) according to manufacturer's instructions. After extensive washing, additional primary antibodies were added overnight at 4 °C. After another round of washing, goat anti-mouse Alexa 488, donkey anti-rabbit or anti-mouse Alexa 546, and streptavidin Alexa 647 (1/500, Invitrogen) were used to detect all three antibodies. To use three primary murine antibodies, slides were blocked with 5.0 μg/mL mouse IgG1 and IgG2a (BioLegend) for 30 min after detection of the first primary antibody with anti-mouse Alexa 647. Slides were then incubated with two primary antibodies directly conjugated to either FITC or Cy3 for 3 h, washed, and incubated with goat anti-FITC Alexa 488 (Invitrogen). Slides were mounted with ProLong Gold with DAPI anti-fade mounting medium (Invitrogen) overnight, and images were acquired by using a LSM510 Confocal Laser Scanning Microscope (Carl Zeiss).

Real-Time PCR. Culture and exposure of human BC cell lines to CTX agents was performed as described (1). mRNA was isolated from cells by using the RNeasy mini kit (Qiagen), contaminating DNA was removed by DNase I (Invitrogen) digestion, and reverse transcription into cDNA was performed by using SuperScript III (Invitrogen) according to the manufactures' directions. Real-time PCR was performed by using the Taqman system after a preamplification step with TaqMan PreAmp (Applied Biosystems) according to the manufacturer's instructions.

1. DeNardo DG, et al. (2011) Leukocyte complexity in breast cancer predicts overall survival and functionally regulates response to chemotherapy. *Cancer Discovery* 1: 54–67.

Fig. S1. Gating strategy for identification of myeloid-lineage populations. Starting from the upper left, arrows indicate directionality of subgates. Markers are indicated to the left and bottom of each polychromatic dot plot. Identified populations are marked in red text.

Fig. S2. Gating strategy for identification of lymphocyte populations. Starting from the upper left, arrows indicate directionality of subgates. Markers are indicated to the left and bottom of each polychromatic dot plot. Identified populations are marked in red text.

Fig. S3. Immunofluorescent staining in murine mammary tumors for CD68 (red; *i* and *iii*), CSF1R (green; *i* and *ii*) or F4/80 (red, *ii*; green, *iii*).

Fig. S4. Activation marker expression on T lymphocytes. (*A*) Representative histograms of CD28 expression for CD3$^+$CD4$^+$ (*Upper*) or CD3$^+$CD8$^+$ (*Lower*) T cells isolated from a single CTX-treated patient with both normal (blue) and tumor (red) tissue. (*B* and *C*) Percent of CD69 expressing (*B*) or HLA-DR expressing (*C*) T cells from all samples.
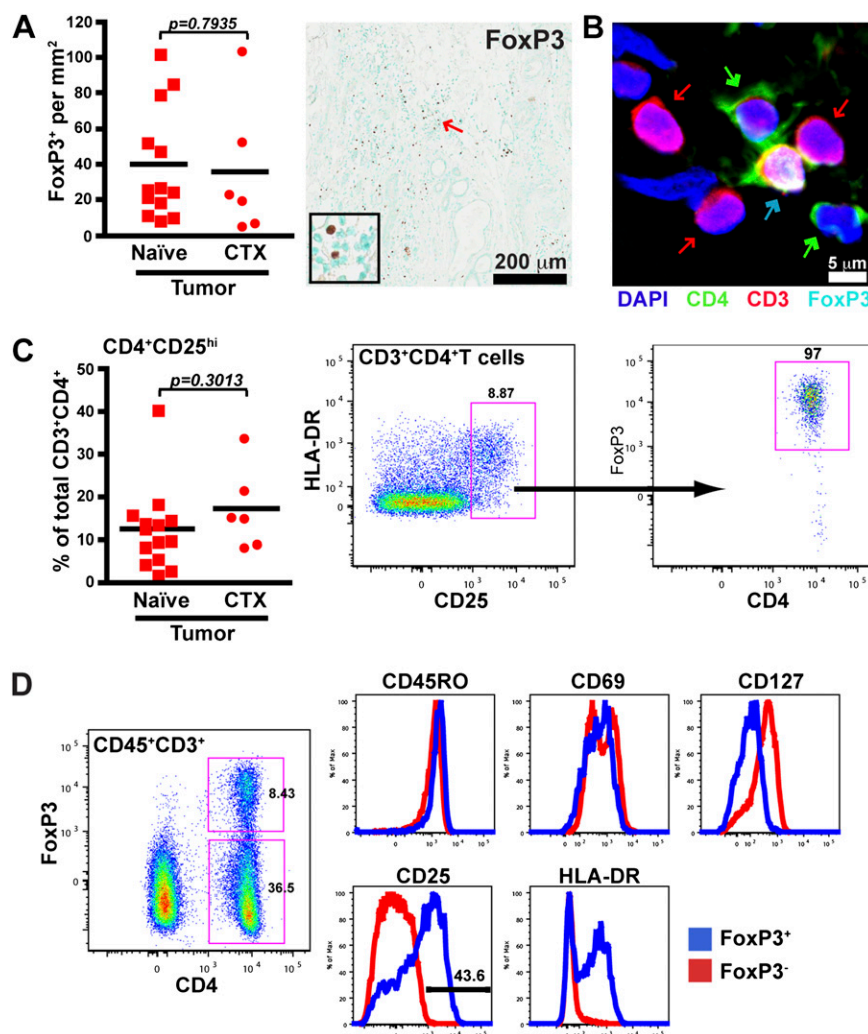
Fig. S5. Presence of CD4+FoxP3+ regulatory T cells within tumors. (*A*) Number of FoxP3 positive cells per area as determined by automated counting (*Left*) with a representative stained section shown (*Right*). (*B*) Immunofluorescent staining of tumors for CD4 (green), CD3 (red), and FoxP3 (teal). Arrows indicate CD3+CD4−FoxP3− (red), CD3+CD4+FoxP3− (green), and CD3+CD4+FoxP3+ (teal) cells. (*C*) Percent of CD25hi cells within the CD3+CD4+ T-cell population (*Left*) with a representative polychromatic dot plot demonstrating FoxP3 staining within this population (*Right*). (*D*) Representative histograms of CD3+CD4+FoxP3− (red) and CD3+CD4+FoxP3+ cells (blue) showing expression of CD45RO, CD69, CD25, CD127, and HLA-DR.

Fig. S6. CTX induces chemokine gene expression changes in human breast cancer cell lines. Relative gene expression compared with untreated controls after in vitro exposure to 25 nM paclitaxel or cisplatin for 24 h. Data represent an average of three replicates. Absence of bars for treated samples indicates undetectable gene expression in control. Fold change of 1× is shown with black horizontal bar, and 2× change is shown with gray horizontal bar.

Table S1. Patient information for evaluated tissue samples. ER, PR, and Her2 status is shown as grade, with percent positivity for ER/PR, and Her2 (evaluated by FISH) shown in parentheses

Age	Histology	Grade	ER	PR	Her2	Tumor size, cm	Node	Neoadjuvant Therapy
63	IDC	3	0 (0)	0 (0)	0 (1.1)	1.6	−	None
56	IDC	3	3+ (95)	3+ (90)	0	2.6	+	None
57	IDC	2	3+ (99)	2–3+ (25)	0	0.9	+	None
61	IDC	3	3+ (99)	3+ (60)	2+ (1.0)	4.8	+	None
78	IDC	3	3+ (30)	1–3+ (40)	3+	2.2	+	None
54	ILC	2	3+ (30)	3+ (30)	0	7.0	+	None
78	IDC	3	3+ (100)	0 (0)	2+ (1.0)	2.2	−	None
55	ILC	3	3+ (95)	0 (0)	2+ (1.6)	7.3	+	None
76	IDC	2	0 (0)	0 (0)	2+ (1.2)	5.1	−	None
65	IDC	2	1–3+ (90)	1–3+ (60)	0	9.0	+	None
74	IDC	2	1+ (1)	0 (0)	2+ (−)	0.8	+	None
65	ILC	2	3+ (100)	1–3+ (60)	0	1.1	−	Tamoxifen
59	ILC	2	3+ (100)	1+ (10)	0	7.0	+	None
71	ILC	1	3+ (95)	0 (0)	0	3.0	−	None
73	IDC	2	3+ (100)	2–3+ (50)	3+	9.8 (4.2)	+ (+)	Docetaxel, Carboplatin, Trastuzumab
66	IDC	3	0 (0)	0 (0)	0 (1.7)	10 (9.6)	+ (+)	Valproic Acid, 5-FU, Epirubicin, Cyclophosphamide
49	IDC	3	3+ (90)	0 (0)	2+ (2.3)	4.3 (4.3)	− (−)	Paclitaxol, Doxorubicin, Cyclophosphamide
39	IDC	2	3+ (95)	0 (0)	2+ (1.1)	8.0 (9.9)	+ (+)	Docetaxel, Doxorubicin, Cyclophosphamide
38	IDC	2	0 (0)	0 (0)	3+	3.5 (9.2)	+ (+)	Doxorubicin, Cyclophosphamide, Trastuzumab, Lapatinib
51	IDC	3	2+ (20)	0 (0)	2+ (1.0)	3.9 (4.2)	− (−)	Valproic Acid, 5-FU, Epirubicin, Anastrozole

Tumor size and node status are shown following neoadjuvant CTX in parentheses.

Table S2. Antibodies used for flow cytometry

Antigen	Clone	Fluorophore	Company	Catalog no.
CD3ε	OKT3	PerCP-eFluor 710	eBioscience	46-0037-42
CD3ε	OKT3	PerCP-Cy5.5	eBioscience	45-0037-42
CD4	RPA-T4	Qdot 655	Invitrogen	Q10007
CD4	RPA-T4	PE	BioLegend	300508
CD8α	RPA-T8	APC-eFluor 780	eBioscience	47-0088-42
CD8α	RPA-T8	Qdot 605	Invitrogen	Q10009
CD11b	ICRF44	PE-Cy7	eBioscience	25-0118-42
CD11c	3.9	Alexa 700	eBioscience	56-0116-73
CD14	61D3	Qdot 655	Invitrogen	Q10056
CD15	W6D3	Alexa 647	BioLegend	323012
CD19	HIB19	Alexa 700	eBioscience	56-0199-73
CD19	HIB19	PerCP-Cy5.5	eBioscience	45-0199-73
CD20	2H7	Alexa 700	BioLegend	302322
CD20	2H7	PerCP-Cy5.5	BioLegend	302326
CD25	BC96	PE-Cy5	BioLegend	302608
CD25	BC96	PE-Cy7	eBioscience	25-0259-42
CD27	O323	Alexa700	eBioscience	56-0279-73
CD28	CD28.2	PE-Cy7	eBioscience	25-0289-42
CD45	HI30	Qdot 705	Invitrogen	Q10062
CD45	HI30	APC-780	eBioscience	47-0459-42
CD45RA	HI100	Qdot 605	Invitrogen	Q10047
CD45RO	UCHL1	Alexa700	BioLegend	304218
CD49d	9F10	PE-Cy5	BioLegend	304306
CD56	HCD56	PE-Cy5	BioLegend	318308
CD56	HCD56	PerCP-Cy5.5	BioLegend	318322
CD69	FN50	FITC	eBioscience	11-0699-73
CD85g	17G10.2	APC	eBioscience	17-5179-42
CD86	IT2.2	PE-Cy5	eBioscience	15-0869-73
CD117	YB5.B8	PE	eBioscience	12-1179-42
CD127	eBioRDR5	650NC	eBioscience	95-1278-42
CCR4	TG6	PE-Cy7	BioLegend	335405
CCR5	HEK/1/85a	PE	BioLegend	313708
CCR7	TG8	Alexa 647	BioLegend	335603
CXCR3	TG1	Alexa 647	BioLegend	334903
FcεR1	AER-37	FITC	eBioscience	11-5899-73
FoxP3	PCH101	PE-Cy5	eBioscience	15-4776-42
HLA-DR	L243	eFluor450	eBioscience	48-9952-42
γδ TCR	B1.1	Alexa 647	BioLegend	331214
Vα24Jα18	6B11	PE	eBioscience	12-5806-42

Table S3. Antibodies used for immunohistochemistry and immunofluorescence

Antigen	Species	Dilution	Company	Catalog no.
CD3	Rabbit	1/150	Thermo Scientific	RM-9107-S1
CD4	Mouse	1/20	Thermo Scientific	MS-1528-S1
CD8	Mouse	1/100	Thermo Scientific	MS-457-S1
CD20	Mouse	1/50	Abcam	Ab9475
CD31 FITC	Mouse	1/10	BioLegend	303104
CD45	Mouse	1/100	eBioscience	14–0459-82
CD45 FITC	Mouse	1/10	BioLegend	304003
CD68	Mouse	1/100	Thermo Scientific	MS-397-P
CSF1R	Rabbit	1/100	Abcam	61137
Pan-keratin Alexa 488	Mouse	1/100	Cell Signaling	4523
FoxP3	Mouse	1/40	eBioscience	14-4777-82
Granzyme B	Mouse	1/50	Thermo Scientific	MS-1157-S1